

# Revisiting compressible and incompressible pressure-strain interaction in kinetic plasma turbulence

Subash Adhikari,<sup>1</sup> Yan Yang (杨艳),<sup>1</sup> and William H. Matthaeus<sup>1</sup>

*Department of Physics and Astronomy, University of Delaware, Newark, DE 19716, USA*

(\*Electronic mail: subash@udel.edu)

In this study, we revisit the pressure-strain interaction in kinetic turbulence, and in particular we re-examine the decomposition of pressure-strain interaction into compressive and incompressive parts. The pressure dilatation ingredient is clearly due to plasma compressions, but here using kinetic particle-in-cell (PIC) simulations of plasma turbulence, it is demonstrated that the remaining anisotropic part, often called Pi-D, also contains contributions due to compressive, non solenoidal velocities of the particle species. The compressive Pi-D can play a significant role in systems with low plasma  $\beta$  even if the system starts with small density variations. The compressive ingredient of Pi-D is found to be anticorrelated with both incompressive Pi-D and pressure dilatation.

## I. INTRODUCTION

Investigation of dissipation mechanisms in collisionless plasma turbulence has been an active area of study for decades. However, in recent years it has become recognized that the conversion of macroscopic (fluid) motions into internal energy must pass through the channel denoted as *pressure-strain interaction*<sup>1,2</sup>. Considerations of pressure-strain interaction have emphasized its distinct role, relative to, for example the electromagnetic work<sup>2,3</sup>, that can convert magnetic energy into species flow energy, or heat conduction, that transports internal energy across space. Instead it is a rigorous consequence of Vlasov Maxwell theory that pressure-strain interaction is the energy transfer channel that converts energy from flow to thermal degrees of freedom. In addition to the elementary decomposition that separates pressure dilatation and Pi-D (see below), different types of decomposition have been proposed in Cassak and Barbhuiya<sup>4</sup>. Here we revisit the decomposition of the pressure-strain interaction in kinetic plasma, and explore how this changes our previous understanding of pressure-strain interaction, and in particular its elements that may be described as incompressive and compressive.

The pressure-strain interaction (P:S) for any plasma species  $\alpha$  can be decomposed as follows:

$$\underbrace{-(\mathbf{P}_\alpha \cdot \nabla) \cdot \mathbf{u}_\alpha}_{\text{P:S}_\alpha} = \underbrace{-p_\alpha \nabla \cdot \mathbf{u}_\alpha}_{p\theta_\alpha} - \underbrace{\Pi_\alpha : \mathbf{D}_\alpha}_{\text{Pi-D}_\alpha}, \quad (1)$$

where  $p_\alpha = P_{\alpha,ii}/3$  is the scalar pressure,  $\Pi_{\alpha,ij} = P_{\alpha,ij} - p_\alpha \delta_{ij}$  is the deviatoric part of the pressure tensor,  $D_{ij,\alpha} = (\partial_i u_{j,\alpha} + \partial_j u_{i,\alpha})/2 - (\nabla \cdot \mathbf{u}_\alpha) \delta_{ij}/3$  is the traceless symmetric part of the velocity gradient with  $\mathbf{u}_\alpha$  being the velocity of species  $\alpha$ . Note that  $p\theta_\alpha$  and  $\text{Pi-D}_\alpha$  denote the isotropic and anisotropic part of the pressure-strain interaction  $\text{P:S}_\alpha$  respectively. This decomposition was previously referred to as the compressive  $p\theta_\alpha$  and incompressive  $\text{Pi-D}_\alpha$  ingredients of the pressure-strain interaction.

It is clear that  $p\theta_\alpha$  arises from compression. Following the standard nomenclature in neutral gas dynamics, we denote this term as the pressure-dilatation. Here we will identify and quantify other contributions to pressure-strain interaction due to plasma compression. While it is not trivial to quantify the effects of compression on the pressure tensor itself, the path

to separation of compressive effects due to the velocities is quite straightforward. One can perform a Helmholtz decomposition<sup>5</sup> and separate the velocity  $\mathbf{u}_\alpha$  for each species  $\alpha$  field into irrotational  $\mathbf{u}^c$  (compressive) and solenoidal  $\mathbf{u}^s$  components i.e.  $\mathbf{u} = \mathbf{u}_\alpha^s + \mathbf{u}_\alpha^c$  such that  $\nabla \cdot \mathbf{u}^c = 0$  and  $\nabla \times \mathbf{u}^c = 0$ . Now the traceless symmetric part of the velocity gradient  $\mathbf{D}_\alpha$  can be further decomposed into compressive and incompressive parts:

$$\mathbf{D}_\alpha = \mathbf{D}_\alpha^c + \mathbf{D}_\alpha^s \quad (2)$$

which immediately implies the decomposition

$$\text{Pi-D}_\alpha = \text{Pi-D}_\alpha^c + \text{Pi-D}_\alpha^s, \quad (3)$$

which makes it explicit that  $\text{Pi-D}_\alpha$  consists of both an incompressive contribution  $\text{Pi-D}_\alpha^s$  and a compressive contribution  $\text{Pi-D}_\alpha^c$ .

It is shown that the compression effect is present in not only the pressure-dilatation term but also the anisotropic part of the pressure-strain interaction  $\text{Pi-D}_\alpha$ , which merits more attention. We should note in passing that the same decomposition of flow velocities can be carried out in magnetohydrodynamics (MHD), resulting in an analogous contrast between dissipation due to compressive flows and due to solenoidal flows<sup>6-9</sup>. Of course in the MHD gas dynamics case, the dissipation functions are expressed in terms of collisional closures, thus obscuring the underlying role of pressure strain. In the present paper, we proceed to examine, for the collisionless plasma case, the compressive and incompressive contributions of  $\text{Pi-D}_\alpha$  for electrons ( $\alpha = e$ ) and ions ( $\alpha = i$ ) in more detail, with the aim to correct our previous understandings on  $\text{Pi-D}_\alpha$ .

## II. SIMULATIONS

In this study we use fully kinetic PIC simulations of turbulence employing the P3D code<sup>10</sup>. The simulations are performed in a two dimensional X-Y plane with all three components of the field vectors but no variation along the out-of-plane Z direction. In P3D, a standard set of normalization is used largely based on protons, with number density normalized to a reference value  $n_r$ , mass normalized to proton mass  $m_i$ , charge normalized to proton charge  $e$ , and magnetic field normalized to a reference field  $B_r$ . Length is normalized to

the proton inertial length  $d_i$ , time normalized to the proton cyclotron time  $\omega_{ci}^{-1}$ , and velocity is normalized to the equivalent reference Alfvén speed  $V_{Ar} = B_r / (\mu_0 m_i n_r)^{1/2}$ .

The simulations are performed in a square periodic domain of size  $L = 150 d_i$  with  $4096^2$  spatial grid points. For numerical expediency both simulations employ artificially low values of the proton to electron mass ratio,  $m_i/m_e = 25$ , and the speed of light,  $c = 15 V_{Ar}$ . We use a total of 3200 particles of each species per cell ( $\sim 10^{11}$  total particles). The system is a decaying initial value problem, starting with uniform densities and temperatures for both species. A uniform magnetic field,  $B_0 = 1.0$ , is directed normal to the plane, in the  $Z$  direction. The initial velocity  $\mathbf{u}$  and magnetic  $\mathbf{B}$  fluctuations are transverse to  $B_0$  (corresponding in linear theory to a small amplitude ‘‘Alfvén mode’’), populating Fourier wavevectors  $2 \leq |\mathbf{k}| \leq 4$  with random phases and prescribed amplitudes. The initial fluctuation energy, flow plus magnetic, is  $E = 0.1$ , and the normalized cross helicity  $\sigma_c$  is negligible. We vary the electron and proton temperatures to change the plasma beta, ratio of the thermal pressure to the magnetic pressure. Results from four simulations with ion and electron plasma beta  $\beta_i = \beta_e = (0.03, 0.3, 0.6, 1.2)$  are presented in this study. For the  $\beta = 0.03$  case, the grid scale is reduced to half compared to the other cases to account for the reduced electron gyroscale. Also for convenience, we drop the subscript  $i$  and  $e$  with the understanding that  $\beta$  represents plasma beta of individual species.

### III. RESULTS

In Fig. 1a we show the time evolution of the plasma compressibility ratio  $C_p = (\langle \delta n^2 \rangle / \langle n \rangle^2) / (\langle \delta B^2 \rangle / \langle B \rangle^2)$ , where  $\delta n$  is the root mean square (rms) density fluctuation and  $\delta B$  is the rms fluctuation in the magnetic field. Note that all the simulations have been initialized with the same density fluctuation of  $\delta n / \langle n \rangle = 0.01178$ . For the simulation with the lowest  $\beta$ , the fluctuation  $\delta n / \langle n \rangle$  increases to 0.25 as the system evolves. In the highest  $\beta$  case,  $\delta n / \langle n \rangle$  increases to about 0.05. The measure of compressibility employed is through the compressibility ratio  $C_p$  accounting for the possible anti-correlation between density and magnetic field<sup>11</sup>. Initially all runs have  $C_p = 10^{-3}$ , and this increases in time as turbulence develops. In particular, it is found that the compressibility ratio  $C_p$  achieves larger values for simulations with smaller  $\beta$ . For the  $\beta = 1.2$  case,  $C_p$  saturates at about  $2 \times 10^{-2}$  while for  $\beta = 0.03$ ,  $C_p$  increases to about 0.6. This implies that, especially for low  $\beta$  cases, even though the simulations start with an incompressible initial condition, compressibility effects can be significant as the system evolves.

Fig. 1b shows the time evolution of the Alfvén ratio  $R_A = \langle \delta V_i^2 \rangle / \langle \delta B_A^2 \rangle$ , where  $\delta V_i$  is the ion-velocity fluctuation amplitude and  $\delta B_A$  is the amplitude of the magnetic field ( $\mathbf{B}$ ) fluctuation in Alfvén units i.e.  $\mathbf{B}_A = \mathbf{B} / \sqrt{4\pi m_i n_i}$  with  $m_i$  and  $n_i$  being the mass and number density of ions respectively. Initially, the velocity and magnetic field fluctuation energies are equal. As the system evolves, the fluctuation in magnetic field dominates over the velocity field. While this ratio is almost

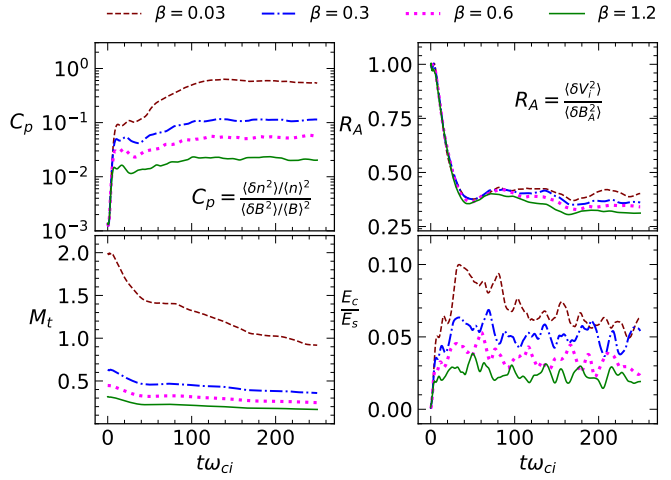


FIG. 1. Time evolution of the plasma compressibility ratio  $C_p$ ; Alfvén ratio  $R_A$ ; turbulent Mach number  $M_t$ ; and the ratio of the total (ions plus electrons) compressible flow energy  $E_c$  to solenoidal flow  $E_s$  energy.

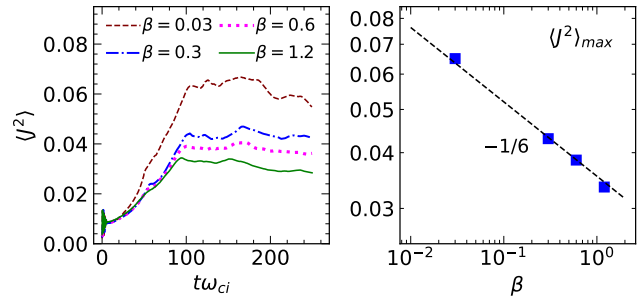


FIG. 2. Left: Time evolution of the mean square current  $\langle J^2 \rangle$  in all the runs. Right: Scaling the plateau of the maximum mean square current as a function of beta  $\beta$ . A line of slope  $-1/6$  is drawn for reference.

independent of plasma  $\beta$  until about  $t\omega_{ci} = 40$ , at later times systems with larger  $\beta$  values show smaller Alfvén ratios.

Fig. 1c shows the time evolution of the turbulent Mach number  $M_t = \delta u / c_s$ , where  $\delta u$  is the root mean square (r.m.s) ion velocity fluctuation and  $c_s$  is the sound speed estimated using ion temperature. Among all the systems, only the lowest beta case  $\beta = 0.03$  has  $M_t > 1$  which falls off rapidly compared to the other cases and goes below unity at late times. Fig. 1d shows the evolution of the ratio of the total (ion plus electron) compressible to incompressible flow energy  $E_c/E_s$  defined as  $E_{c,\alpha} = \frac{1}{2} \langle \rho_\alpha | \mathbf{u}_\alpha^c |^2 \rangle$  and  $E_{s,\alpha} = \frac{1}{2} \langle \rho_\alpha | \mathbf{u}_\alpha^s |^2 \rangle$  for each species  $\alpha$  with mass density  $\rho_\alpha$ . This quantity is greatest throughout the run for the  $\beta = 0.03$  case, and the ordering progresses to lower values for the respective higher  $\beta$  cases, which is consistent with the trends in Fig. 1a and c.

In Fig. 2a we compare the time evolution of the mean square current  $\langle J^2 \rangle$  in all four cases. Initially, the mean square current oscillates in all the simulations with the amplitude of

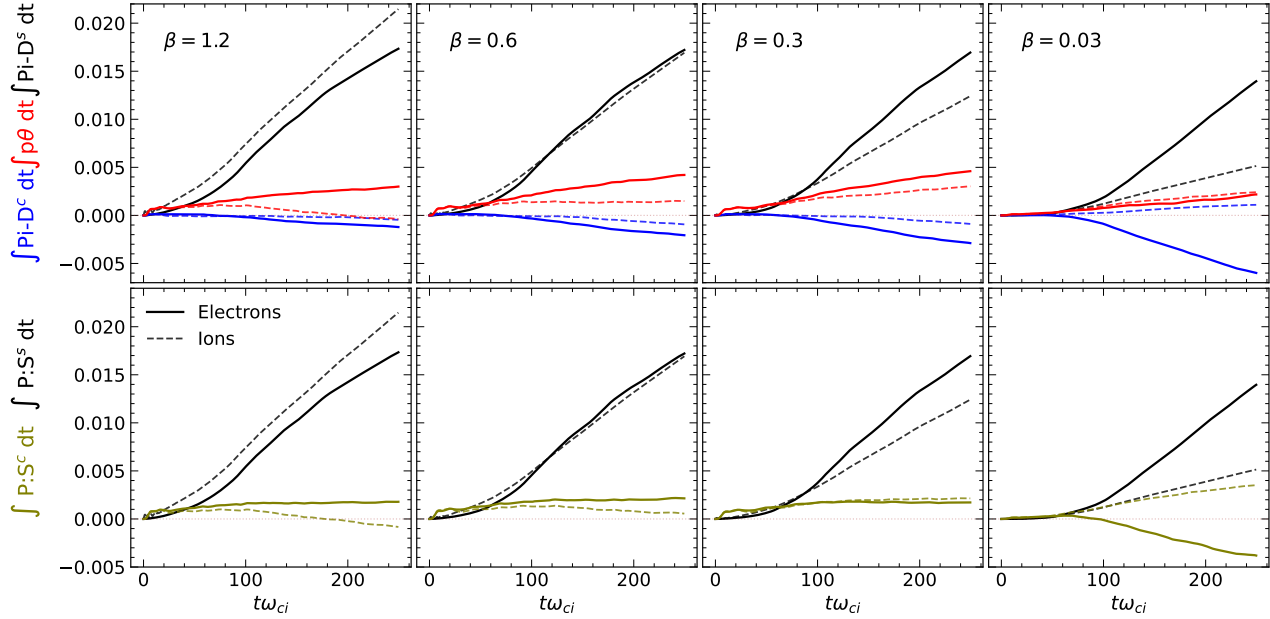


FIG. 3. Top panel: Time evolution of the cumulative time integral of the compressible and incompressible contribution of Pi-D along with the cumulative integral of  $p\theta$  for both ions (dashed lines) and electrons (solid lines) for different plasma beta. Bottom Panel: Time evolution of the compressible and incompressible contributions to the pressure-strain interaction. Here, the sum of  $Pi \cdot D^c$  and  $p\theta$  represents the compressible contribution to the pressure-strain interaction while  $Pi \cdot D^s$  represents the incompressible contribution.

the current decreasing with a higher value of  $\beta$ . This should be viewed as a startup transient<sup>12</sup>. Following  $t\omega_{ci} = 25$ , the mean square current for the  $\beta = 0.03$  case increases rapidly relative to other cases. The other simulations follow each other closely until  $t\omega_{ci} = 90$  before attaining slightly differing plateaus, once again ordered by their  $\beta$  values. The value of the mean square current around the plateau is shown in Fig. 2b as a function of  $\beta$ . We find the empirical result that the maximum mean square current decreases with higher value of beta as  $\langle j^2 \rangle_{max} \sim \beta^{-1/6}$ . We know of no obvious explanation for this empirical result.

Next, in Fig. 3 we examine the cumulative time integrals of pressure-strain interaction. This represents the net dissipation through the corresponding pathway to internal energy production. In the upper panel, we show the cumulative time integral of the solenoidal and compressible Pi-D named as  $Pi \cdot D^s$  (black curve) and  $Pi \cdot D^c$  (blue curve), respectively. The upper panels also show pressure dilatation, named as  $p\theta$  (red curve) for both ions (dashed lines) and electrons (solid lines). For  $\beta = 1.2$  case, the time integral of  $Pi \cdot D_i^s > Pi \cdot D_e^s$ , and for  $\beta = 0.6$  case, the cumulative integrals  $Pi \cdot D_i^s \simeq Pi \cdot D_e^s$ . For the lower  $\beta$  cases, the time integral of  $Pi \cdot D_e^s$  dominates that of  $Pi \cdot D_i^s$ . The integral of the compressible part of Pi-D for ions is small and negative for all but  $\beta = 0.03$  case. However, the time integral of  $Pi \cdot D^c$  for electrons is always negative with the amplitude increasing with decreasing  $\beta$ . The amplitude of the time integral of  $Pi \cdot D^c$  for electrons is always larger than that of ions, in particular, the electron contribution dominates the ions for  $\beta = 0.03$ .

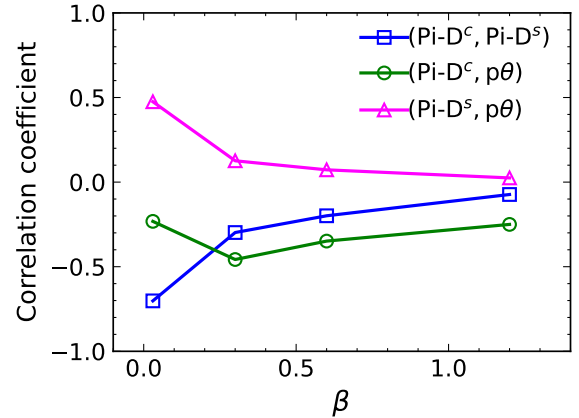


FIG. 4. Correlation coefficient between(a) compressible and incompressible Pi-D (blue squares), (b) compressible Pi-D and  $p\theta$ (green circles), and (c) incompressible Pi-D and  $p\theta$  (magenta triangles) measured for electrons at  $t\omega_{ci} = 150.5$  as a function of  $\beta$ .

The well-known pressure dilatation also incorporates the compression effect. As shown in Fig. 3, the cumulative integral of  $p\theta$  for ions decreases as the system passes the maximum mean square current for  $\beta = 1.2$ , stays almost flat for  $\beta = 0.6$ , and increases for  $\beta = 0.3$ . For the lowest value  $\beta = 0.03$ , the integral of  $p\theta_i$  continues to increase; however, its amplitude remains less than  $p\theta_i$  for the  $\beta = 0.3$  case. Note

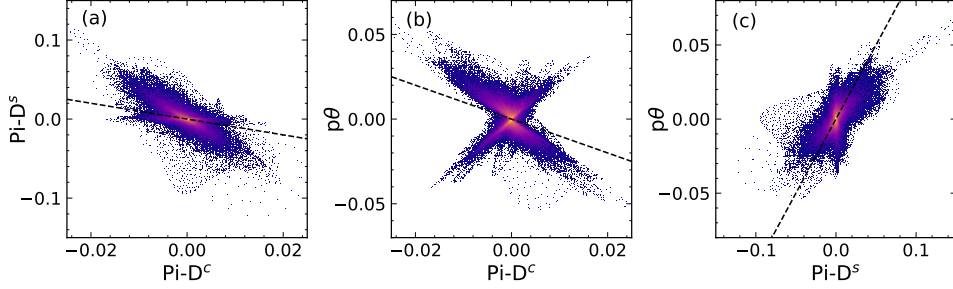


FIG. 5. Joint pdf of (a) compressible and incompressible contributions to  $\text{Pi-D}$  (left), (b)  $p\theta$  and compressible  $\text{Pi-D}$  (middle) and (c)  $p\theta$  and incompressible  $\text{Pi-D}$  for electrons in the system with  $\beta = 0.03$  at  $t\omega_{ci} = 150.5$ . A line of slope  $-1$  is drawn for reference in the left and middle panel while a line of slope  $1$  is drawn on the rightmost plot.

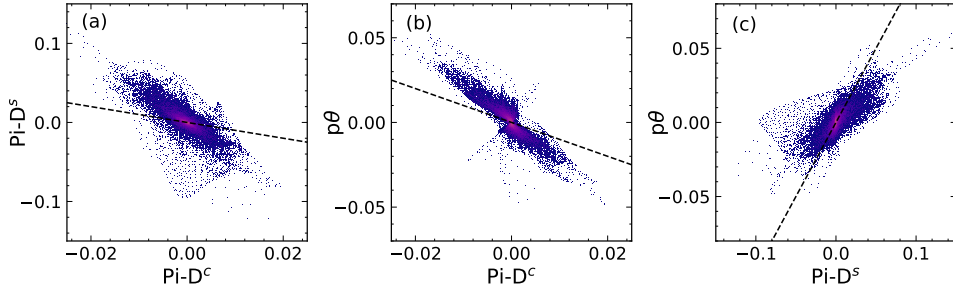


FIG. 6. Same as Fig. 5 but conditioned over regions where the magnitude of the out-of-plane current density  $j_z$  exceeds  $0.75$ .

that the time integral of  $p\theta_e$  is larger than that of ions for  $\beta = 1.2, 0.6, 0.3$  with their differences decreasing with decreasing  $\beta$ . For  $\beta = 0.03$ , the time integral of  $p\theta_i$  exceeds that of electrons.

Next, in the lower panel of Fig. 3, we combine the compressive contributions to the pressure-strain interaction i.e. the sum of  $\text{Pi-D}^c + p\theta \equiv \text{P:S}^c$ , and compare this with the time evolution of the incompressive contribution  $\text{Pi-D}^s \equiv \text{P:S}^s$  for electrons and ions. A subtle but potentially significant feature of the analysis in Fig. 3 is that the compressive contribution  $\text{Pi-D}^c$  is always negative for electrons and almost always negative for protons, except at the highest  $\beta$ . When this occurs, the compressive ‘‘correction’’ to  $\text{Pi-D}$  is, in effect, canceling part of the pressure dilatation.

To further examine this phenomenon, in particular for electrons, in Fig. 4, we plot the correlation coefficient between different contributions to the electron pressure-strain interaction at  $t\omega_{ci} = 150.5$  as a function of  $\beta$ . Note that at this time all the systems are in the plateau of the mean square current (see Fig. 2). As seen in Fig. 4, the compressible and incompressible parts of  $\text{Pi-D}$  shown in blue squares become more anticorrelated as  $\beta$  decreases with  $\beta = 0.03$  case having a correlation coefficient of  $r = -0.70$ . While the correlation between  $\text{Pi-D}^c$  and  $p\theta$  (red circles) stays negative for all values of  $\beta$ , it decreases as  $\beta$  decreases from 1.2 to 0.3, but for  $\beta = 0.03$  the correlation coefficient increases. The correlation between  $\text{Pi-D}^s$  and  $p\theta$  (magenta triangles) is positive for all

cases with the correlation increasing for decreasing  $\beta$ . Since the measure of the anticorrelation between  $\text{Pi-D}^c$  and  $\text{Pi-D}^s$ , and the correlation between  $\text{Pi-D}^s$  and  $p\theta$  is maximum for the lowest  $\beta$  case, we focus on this system and explore the associated probability distribution functions.

In Fig. 5, we examine specifically pairwise local correlations between several contributions to pressure strain for the  $\beta = 0.03$  case. We plot joint probability distribution functions (pdfs) for  $\text{Pi-D}^s$  vs  $\text{Pi-D}^c$ , for  $p\theta$  vs  $\text{Pi-D}^c$ , and for  $p\theta$  vs  $\text{Pi-D}^s$ . For convenience, reference dashed lines of slope  $-1$  and  $+1$  are plotted. From Fig. 5a, it is clear that the compressible and incompressible  $\text{Pi-D}$  have a joint pdf favoring a negative correlation. For compressible  $\text{Pi-D}$  and pressure dilatation, the joint pdf in Fig. 5b shows mixed correlations. Most of the points align to the line of anticorrelation, but there is a lesser population that exhibits positive correlations. It is also clear from Fig. 5c that the incompressible  $\text{Pi-D}$  shows a very strong (positive) correlation with the pressure dilatation  $p\theta$  even though there are some tails deviated from the perfect correlation line.

To understand these correlations better, we isolate the regions with strong out-of-plane current density  $|j_z|/j_{rms} > 0.75$  and Fig. 6 shows the joint pdfs corresponding to these strong current regions. In this case, the arms-like extensions observed in Fig. 5 are largely absent. As a result, the correlation aligns better with the lines drawn for reference. For convenience, we compare the value of the correlation coefficients

TABLE I. Correlation coefficients between different contributions to the electron pressure-strain interaction conditioned on the amplitude of the normalized out-of-plane current  $j_z$ .

Regions	Pi-D <sup>c</sup> , Pi-D <sup>s</sup>	Pi-D <sup>c</sup> , pθ	Pi-D <sup>s</sup> , pθ
$ j_z  > 0.75$	-0.79	-0.88	0.71
$ j_z  < 0.75$	-0.69	-0.16	0.45
All	-0.70	-0.23	0.47

between these pressure-strain elements across regions with different intensities of the out-of-plane current ( $j_z$ ) in Table I. Therefore, in a system with low plasma  $\beta$ , within the localized current sheets, the compressible Pi-D<sup>c</sup> is anti-correlated to both the incompressible Pi-D<sup>s</sup> and pressure dilatation pθ. Even though Pi-D<sup>c</sup> and pθ, both are the compressive contributions to the pressure-strain interaction, the net effect of these quantities is found to be opposite to each other.

#### IV. DISCUSSION AND CONCLUSIONS

In this brief report we revisit the previously discussed decompositions of pressure-strain interaction into compressible and incompressible parts. In earlier work, Pi-D, has been described, either explicitly or implicitly, as the incompressible contribution to the pressure-strain interaction. We report here the elementary, but possibly overlooked, conclusion that when there is a nonuniform irrotational ingredient of the flow, then Pi-D can include a compressible contribution hidden within it. The possibility for this to occur is seen directly from the Helmholtz decomposition of the velocities.

We examine this effect in plasma kinetic (PIC) simulations by directly computing the compressible Pi-D<sup>c</sup> for electrons and ions. The diagnostics examined here have specifically emphasized the intriguing results for electrons. The finding is that the compressible Pi-D<sup>c</sup> can be significant in plasma simulations with low plasma  $\beta$ . Further analysis shows that compressible Pi-D<sup>c</sup> is anticorrelated to the incompressible Pi-D<sup>s</sup> and also is anticorrelated to pressure dilatation pθ when computed over the entire volume. But upon conditioning on current intensity, we find that this anticorrelation is most prominent in regions with strong currents. Because of this anticorrelation, the net compressible contribution to the pressure-strain interaction may differ considerably from the estimate based on pressure dilatation alone. That is, especially for electrons, the newly characterized compressive Pi-D<sup>c</sup> opposes the effect of pressure dilatation. Recognition of this effect calls for revising estimates of the influence of pressure-strain on heating in compressive cases, relative to the standard incompressible heating estimates. Here we see that the globally averaged effect, at low plasma  $\beta$  can be 50% or more for electrons. The local effect, near stronger currents, may be much greater.

As a final word, the potential implications of these results for interpretation of MMS observations are worth mentioning. For example, when one observes  $|p\theta| > |\text{Pi-D}|$  as is often the case in the magnetosheath<sup>13,14</sup>, it is not a necessary conclusion that compressible effects greatly exceed incompressive

dissipation effects. Rather, since we have observed that Pi-D<sup>c</sup> is often anticorrelated with Pi-D<sup>s</sup> and can be large, it may be masking rather large incompressive Pi-D<sup>s</sup> contributions. Alternatively, it is possible that highly compressive flows with very small solenoidal velocity might exhibit significant Pi-D that is of almost fully compressive origin, being dominated by Pi-D<sup>c</sup>. This could be for example a flow consisting of compressional waves and shocklets. Allowing for such possibilities, one should, in general, interpret Pi-D as “incompressive” with great caution. We understand of course that having a full Helmholtz decomposition of the flow would alleviate both of these ambiguities, but this is not available with MMS data in spite of its prodigious capabilities.

#### ACKNOWLEDGMENTS

This research is partially supported by the MMS Theory, Modeling and Data Analysis team under NASA grant 80NSSC19K0565, by the NASA LWS program under grants 80NSSC20K0198 and 80NSSC22K1020, and a subcontract from the New Mexico consortium 655-001, a NASA Heliophysics MMS-GI grant through a Princeton subcontract SUB0000517, and by the National Science Foundation Solar Terrestrial Program grant AGS-2108834. Y.Y. is supported by 2024 Ralph E. Powe Junior Faculty Enhancement Award and the University of Delaware General University Research Program grant. This research was also supported by the International Space Science Institute (ISSI) in Bern, through ISSI International Team projects #556 (Cross-scale energy transfer in space plasmas) and #23-588 (Unveiling energy conversion and dissipation in nonequilibrium space plasmas). We would like to acknowledge high-performance computing support from Cheyenne (doi:10.5065/D6RX99HX) and Derecho (<https://doi.org/10.5065/qx9a-pg09>) provided by NCAR’s Computational and Information Systems Laboratory, sponsored by the National Science Foundation.

<sup>1</sup>Y. Yang, W. H. Matthaeus, T. N. Parashar, P. Wu, M. Wan, Y. Shi, S. Chen, V. Roytershteyn, and W. Daughton, “Energy transfer channels and turbulence cascade in Vlasov-Maxwell turbulence,” *Phys. Rev. E* **95**, 061201 (2017b).

<sup>2</sup>S. Zenitani, M. Hesse, A. Klimas, and M. Kuznetsova, “New measure of the dissipation region in collisionless magnetic reconnection,” *Physical review letters* **106**, 195003 (2011).

<sup>3</sup>Y. Yang, S. Adhikari, and W. H. Matthaeus, “Electron dissipation and electromagnetic work,” *Journal of Geophysical Research: Space Physics* **129**, e2024JA033105 (2024).

<sup>4</sup>P. A. Cassak and M. H. Barbhuiya, “Pressure–strain interaction. i. on compression, deformation, and implications for pi-d,” *Physics of Plasmas* **29** (2022).

<sup>5</sup>G. B. Arfken, H. J. Weber, and F. E. Harris, *Mathematical methods for physicists: a comprehensive guide* (Academic press, 2011).

<sup>6</sup>S. Sarkar, G. Erlebacher, M. Y. Hussaini, and H. O. Kreiss, “The analysis and modelling of dilatational terms in compressible turbulence,” *Journal of Fluid Mechanics* **227**, 473–493 (1991).

<sup>7</sup>D. A. Donzis and J. P. John, “Universality and scaling in homogeneous compressible turbulence,” *Physical Review Fluids* **5**, 084609 (2020).

<sup>8</sup>C. Li, Y. Yang, W. Matthaeus, B. Jiang, M. Wan, and S. Chen, “Nonuniversality and dissipative anomaly in compressible magnetohydrodynamic turbulence,” submitted to *Physical Review Letters* (2023).

<sup>9</sup>J. P. John, D. A. Donzis, and K. R. Sreenivasan, “Does dissipative anomaly

- hold for compressible turbulence?" *Journal of Fluid Mechanics* **920**, A20 (2021).
- <sup>10</sup>A. Zeiler, D. Biskamp, J. F. Drake, B. N. Rogers, M. A. Shay, and M. Scholer, "Three-dimensional particle simulations of collisionless magnetic reconnection," *Journal of Geophysical Research* **107**, 1230 (2002).
- <sup>11</sup>T. Wang, J. Cao, H. Fu, X. Meng, and M. Dunlop, "Compressible turbulence with slow-mode waves observed in the bursty bulk flow of plasma sheet," *Geophysical Research Letters* **43**, 1854–1861 (2016).
- <sup>12</sup>T. N. Parashar, W. H. Matthaeus, and M. A. Shay, "Dependence of Kinetic Plasma Turbulence on Plasma Beta," *The Astrophysical Journal* **864**, L21 (2018), arXiv:1807.11371 [physics.space-ph].
- <sup>13</sup>Y. Wang, R. Bandyopadhyay, R. Chhiber, W. H. Matthaeus, A. Chasapis, Y. Yang, F. D. Wilder, D. J. Gershman, B. L. Giles, C. J. Pollock, J. Dorelli, C. T. Russell, R. J. Strangeway, R. T. Torbert, T. E. Moore, and J. L. Burch, "Statistical Survey of Collisionless Dissipation in the Terrestrial Magnetosheath," *Journal of Geophysical Research* **126**, e29000 (2021).
- <sup>14</sup>Y. Yang, F. Pecora, W. H. Matthaeus, S. Roy, M. E. Cuesta, A. Chasapis, T. Parashar, R. Bandyopadhyay, D. J. Gershman, B. L. Giles, and J. L. Burch, "Quantifying the agyrotropy of proton and electron heating in turbulent plasmas," *The Astrophysical Journal* **944**, 148 (2023).